Amino Acid Side Chain Interactions in the Presence of Salts

Sergio A. Hassan*

Center for Molecular Modeling, Division of Computational Bioscience, National Institutes of Health, U. S. Department of Health and Human Services, Bethesda, Maryland 20892

Received: July 21, 2005; In Final Form: September 9, 2005

The effects of salt on the intermolecular interactions between polar/charged amino acids are investigated through molecular dynamics simulations. The mean forces and associated potentials are calculated for NaCl salt in the 0−2 M concentration range at 298 K. It is found that the addition of salt may stabilize or destabilize the interactions, depending on the nature of the interacting molecules. The degree of (de)stabilization is quantified, and the origin of the salt-dependent modulation is discussed based upon an analysis of solvent density profiles. To gain insight into the molecular origin of the salt modulation, spatial distribution functions (sdf's) are calculated, revealing a high degree of solvent structuredness in all cases. The peaks in the sdf's are consistent with long-range hydrogen-bonding networks connecting the solute hydrophilic groups, and that contribute to their intermolecular solvent-induced forces. The restructuring of water around the solutes as they dissociate from close contact is analyzed. This analysis offers clues on how the solvent structure modulates the effective intermolecular interactions in complex solutes. This modulation results from a critical balance between bulk electrostatic forces and those exerted by (i) the water molecules in the structured region between the monomers, which is disrupted by ions that transiently enter the hydration shells, and (ii) the ions in the hydration shells in direct interactions with the solutes. The implications of these findings in protein/ligand (noncovalent) association/dissociation mechanisms are briefly discussed.

Introduction

Biopolymers such as proteins and nucleic acids are the basic components of biological systems. Their dynamics, conformations, and interactions in the cell determine the behavior of living organisms. Many of the physical and chemical properties of these molecules have been studied using experimental and computational techniques. However, important processes underlying biological function, such as protein−ligand interactions, molecular recognition, aggregation, and protein folding, are not yet well understood. Biomolecular interactions, either in vivo or in vitro, occur mainly in aqueous environments that may vary broadly in composition. Solvents not only affect the conformation, dynamics, and thermodynamics of biomolecules[1,2] but also modulate their chemical properties.[3] In proteins, the solvent controls chemical reactions, e.g., in enzyme catalysis, and modulates noncovalent interactions, thus governing the dynamics of molecular association and dissociation.[4−6] The addition of salts and cosolvents to the solution can cause significant changes in many biomolecular properties.[7−13] For example, protein solubility can change by the addition of salts to the solution.[14] In general, the solubility increases slightly (salting in) at low salt concentrations and drops sharply (salting out) at higher concentrations. Salting out is a common experimental procedure to precipitate proteins and separate them from a solution. The change in protein solubility as well as other properties of proteins in solutions depend on the nature of the salts and cosolvents.[15] Progress has been made in understanding the effects of the Hofmeister series on simple solutes,[16,17] but a clear understanding of their molecular origins in complex solutes has been more elusive. Changing the conditions of the solution can also affect the thermodynamics of single proteins, altering their structural stability.[10,13] Thus, protein denaturation is promoted by changing the concentrations of alcohols, urea, and guanidine hydrochloride, while protein stabilization can be reinforced with the addition of sucrose, certain amino acids, and salts.

Because salts and other electrolytes are ubiquitous in biological systems, understanding their effects on proteins behavior at the molecular level is important to quantify their interactions in a biological or experimental context. Because of the complex nature of these interactions, they do not lend themselves readily to theoretical approximations. Therefore, molecular dynamics (MD) simulations can be used to explore the microscopic origin of such interactions. MD simulations have been used to investigate physical and chemical properties of liquids[18−20] and to study biomolecular processes at an atomic level of detail.[21,22]

Bulk electrostatic modulation of molecular interactions originates in the polarization and reorientation of water molecules in the bulk phase. Protein electrostatics is an important component of intermolecular interactions[23,24] and may determine protein−ligand association and binding free energies.[25,26] Proteins known to interact mainly by electrostatic forces have been engineered to accelerate the rate of association and the formation of tighter molecular complexes.[27,28] Besides bulk electrostatics, other solvent-induced forces (SIFs) result from the rearrangement of water molecules around the solute due to their exclusion from the region occupied by the solute itself.[29,30] This rearrangement modifies (when compared to bulk liquid) the hydrogen-bonding (HB) network of water around the solute, generating forces and torques that affect its equilibrium structure and dynamics. These forces operate regardless of the polar character of the solute; e.g., hydrophobic forces[31−33] are SIFs between nonpolar molecules. Hydrophobic forces make important contributions to protein−ligand binding, are linked to

* Author to whom correspondence should be addressed. Phone: (301) 402-1382. Fax: (301) 402-2867. E-mail: mago@helix.nih.gov.

10.1021/jp054042r
Published on Web 10/28/2005

protein recognition and specificity, and play a role in early protein folding events.[34,35] For polar and charged solutes[36] the rearrangement of the excluded solvent and its HB network is locally perturbed by the electric field. Therefore, the microscopic origin of the SIF is more complex and indirectly affected by the field. In this case the formation of solute−solvent−solute HB may result in so-called hydrophilic forces[37] (i.e., SIF between hydrophilic groups) that may also affect protein−ligand interactions and protein folding.[4,30,38]

Both electrostatics and solvent-induced forces are modified by the presence of salts.[25,26,39−41] A recent study[42] quantified the extent in which salt concentration strengthens the hydrophobic interaction between two methane molecules. For polar and charged solutes bulk electrostatic forces and SIFs operate simultaneously. A systematic study of salt effects on the intermolecular interactions in these systems has not yet been reported and is presented here. Extensive MD simulations are carried out to calculate the intermolecular mean forces (MF) between amino acid pairs and their associated potentials (PMFs) and to quantify the changes induced by the ion atmosphere at different salt concentrations. The molecular origin of such modulations is investigated.

Computational Methods

Structurally simple solutes (e.g., methane molecules) have proven useful in gaining insight into the salt-dependent modulation at the molecular level. A certain degree of structural complexity is desirable, however, to study biomolecular interactions more realistically. Amino acids differ broadly in their topologies and chemical properties and are simple enough for the systematic study sought herein. Thus, eight amino acid dimers were modeled here as described earlier[43] by combining five polar/charged acceptor/donor molecules: Asp^-−Arg^+, Asp^-−Lys^+, Asp^-−His^+, Asp^-−Ser, Ser−Arg^+, Ser−Lys^+, Ser−His^+, and Ser−Ser; a dimer is then defined as two monomers (each monomer being a single amino acid) interacting through noncovalent forces. Details of the computational setup were reported in ref 43; an overview and additional details are given below for completeness. The carboxy and amino termini of each amino acid were capped with uncharged groups. Each dimer was immersed in a cubic box of volume ∼(46 Å)^3, containing TIP3P water molecules at $T = 298$ K and a density of $\rho_w \approx 0.993$ g/cm^3. Salt concentrations of 0.1, 0.5, 1.0, and 2.0 M (mol/L; equal to the ionic strength in this case) are considered; Na^+ and Cl^- ions were introduced by replacing water molecules (one per ion) randomly; additional ions were added to neutralize the system when required.[43] MD simulations were carried out using periodic boundary conditions (PBC) and particle mesh Ewald (PME) summations; the all-atom CHARMM force field was used.[44] The system was initially equilibrated for 1 ns to allow ions to diffuse and accommodate around the solutes at their initial configuration (proton−acceptor distance of 1 Å). The convergence of the spatial distribution of ions was not quantified but assessed by visual inspection of their spatial distribution functions (sdf's; see below). The distance r between the monomers was then increased in successive steps of $\Delta r = 0.2$Å along the line connecting the donor, the shared proton, and the acceptor atoms as described;[43] an equilibration phase of 100 ps followed each distance update to relax local perturbations of the liquid. The production phase comprised a set of successive simulations of $\tau = 240$ ps each, adding up to a total production time of $\tau_T \approx 15$ ns (a 4-fold increase with respect to the simulations in pure water reported previously,[43] and needed here to reduce statistical errors for the comparison of the PMF).

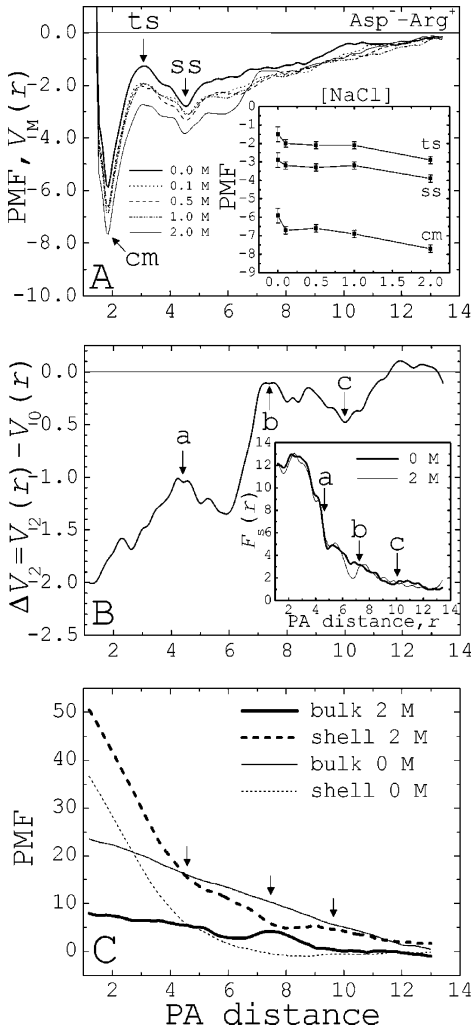

Figure 1. (A) Potentials of mean force (V_M, in kcal/mol) for the Asp^-−Arg^+ dimer as a function of the intermolecular (PA = proton−acceptor, in Å) distance, at different NaCl salt concentrations. Inset: Changes of the potentials at the contact (cm), transition state (ts), and solvent-separated (ss) distances as a function of [NaCl]. (B) Changes (ΔV_2) of the potentials at 2 M salt concentration with respect to the salt-free solvent. Arrows (a, b, and c) mark the approximate intermolecular distances where changes of the PMF occur; these changes coincide with the development of new solvent density maxima in the space between the monomers (see text and Figure 6). Inset: Solvent mean force ($F_{s,M}$, in kcal/mol/Å) for pure water and 2 M solution. (C) Bulk (electrostatics) and nonbulk (solvation-shell) contributions to the PMF as a function of the intermolecular distance, in pure water and 2 M salt concentration.

Results

A one-letter code will be used for the amino acids as follows: R = Arg^+, K = Lys^+, H = His^+, D = Asp^-, and S = Ser. Figure 1A shows the PMF, $V_M(r)$, for the DR dimer at different salt concentrations (indicated by the index M; $V_0(r)$ corresponds to pure water); adding salt stabilizes the intermolecular interaction in this case. The inset in Figure 1A shows $V_M(r)$ at $r = r_{cm}$, r_{ts}, and r_{ss}, corresponding to the contact, transition state (desolvation barrier), and solvent-separated proton−acceptor distances, respectively. At the contact minimum, the dimer stabilizes by ∼1 kcal/mol at 1 M and by ∼2 kcal/mol at 2 M. PMF plots for the SR dimer are presented in Figure 2A, showing the opposite effect of salt, i.e., neutralizing the acceptor molecule destabilizes the interactions; e.g., at 2 M an increase of ∼1 kcal/mol is observed at the contact distance. Adding salt also strengthens the interactions of DS and SS

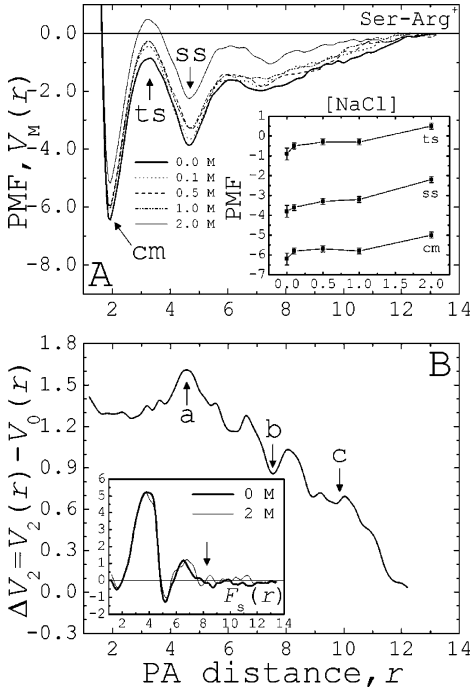

Figure 2. As in Figures 1A and 1B for Ser−Arg^+ (see Figure 7).

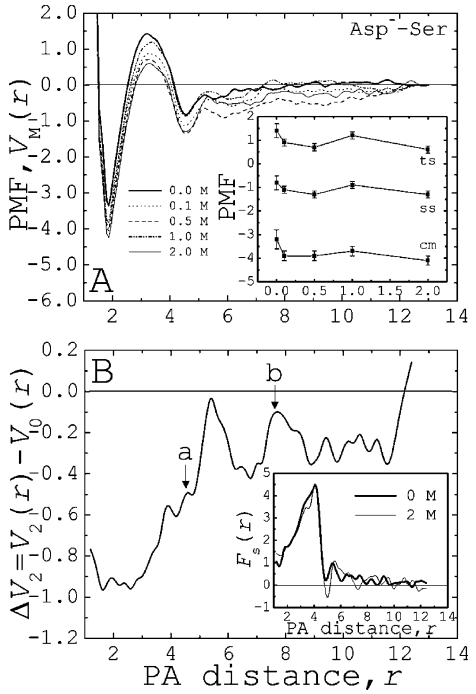

Figure 3. As in Figures 1A and 1B for Asp^-−Ser (see Figure 8).

dimers (cf. Figures 3A and 4A). Figure 5 displays the potentials $V_M(r_{cm})$ with respect to pure water, at different salt concentrations (i.e., $\Delta V_M(r_{cm}) = V_M(r_{cm}) - V_0(r_{cm})$) for the eight dimers studied here; a summary of the calculated values of $\Delta V_M(r)$ at r_{cm}, r_{ts}, and r_{ss} is given in Table 1. Figure 5 shows no obvious correlation between the strength of the (de)stabilization and the polar/charged nature of the monomers. Thus, the interactions between charged species may either stabilize (DR) or destabilize (DK) with added salt or show little variations as in DH. A similar lack of correlation is observed for dimers containing one neutral molecule; SR destabilizes by ∼1 kcal/mol, while SH stabilizes by the same amount at 2 M; adding salt also stabilizes the SS dimer by more than ∼1 kcal/mol at 2 M. These observations suggest that a critical balance of solvent forces

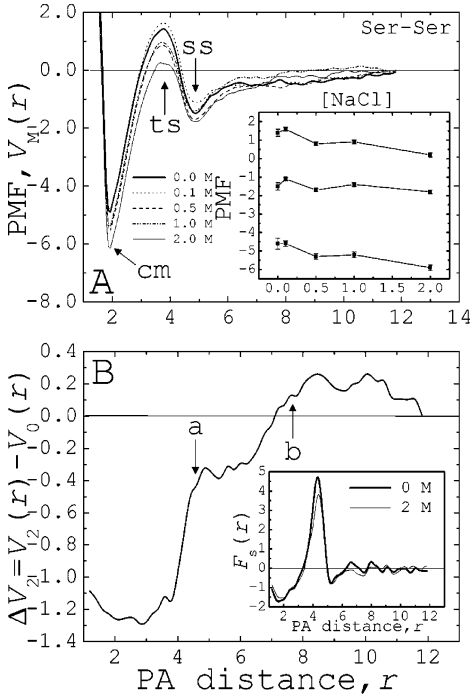

Figure 4. As in Figures 1A and 1B for Ser−Arg^+ (see Figure 7).

may be operating on the solutes in the 0−2 M salt concentration range. It is then of interest to analyze the solvent component, $F_{s,M}(r)$, of the intermolecular mean forces (MFs) for the four representative dimers discussed above as well as their effects on the potentials. As shown in Figure 5, the larger effects of salts are observed at higher concentrations (∼1−2 M), so only the forces and potentials in pure water and in 2 M solution are discussed.

Figure 1B shows the change of the intermolecular potential for the DR dimer in 2 M solution with respect to pure water as a function of the intermolecular distance, i.e., $\Delta V_2(r) = V_2(r) - V_0(r)$. As the intermolecular distance decreases, $\Delta V_2(r)$ decays ∼0.5 kcal/mol above $r \approx 10$ Å (arrow c) and grows again by the same amount at $r \approx 8$ Å (arrow b); $\Delta V_2(r)$ drops sharply (∼1.5 kcal/mol) in the region 6 Å $< r <$ 8 Å, followed by a smaller increment of ∼0.5 kcal/mol up to $r \approx 4.5$ Å (∼r_{ss}, arrow a), where it continues to decrease steadily as the monomers approach the close-contact distance r_{cm}. These up-and-down changes result in an overall downward slope of $\Delta V_2(r)$, which yields a total stabilization of ∼1.8 kcal/mol with respect to the salt-free solution (cf. Figure 5). The inset of Figure 1B shows the mean forces exerted by the solvent in pure water and 2 M concentration; the forces are positive at all distances, which means that they tend to separate the monomers at all distances regardless of the ionic strength. The forces exerted by the solvent are calculated as in ref 43, i.e., $\langle \mathbf{F}_{s,M}(r) \rangle = \langle \mathbf{r}' \cdot \Delta\mathbf{F}(r) \rangle \mathbf{r}'/2$, where $\mathbf{r}'$ is a unit vector along the direction of movement, and $\Delta\mathbf{F}(r) \equiv \mathbf{F}_A(r) - \mathbf{F}_D(r)$, where $\mathbf{F}_i(r)$ is the average force that the solvent exerts on the acceptor (i = A) or donor (i = D) molecules evaluated at their centers of mass, for a proton−acceptor (PA) distance r ($F_{s,M} > 0$, repulsive; $F_{s,M} < 0$, attractive). Figure 1B shows that the variations of $\Delta V_2(r)$ with the distance originate in changes of the relative magnitude of the repulsive forces exerted by the solvent in specific regions; below $r \approx r_{ss}$, $F_{s,2}$ remains smaller than $F_{s,0}$, leading to the slow decay of $\Delta V_2(r)$ in that region; a sudden drop of $F_{s,2}$ in 6 Å $< r <$ 8 Å causes the sharp decay of $\Delta V_2(r)$ and accounts for a large part of the stabilization of the dimer; a damped force is also observed above $r \approx 10$ Å. It is instructive to compare the contributions of bulk

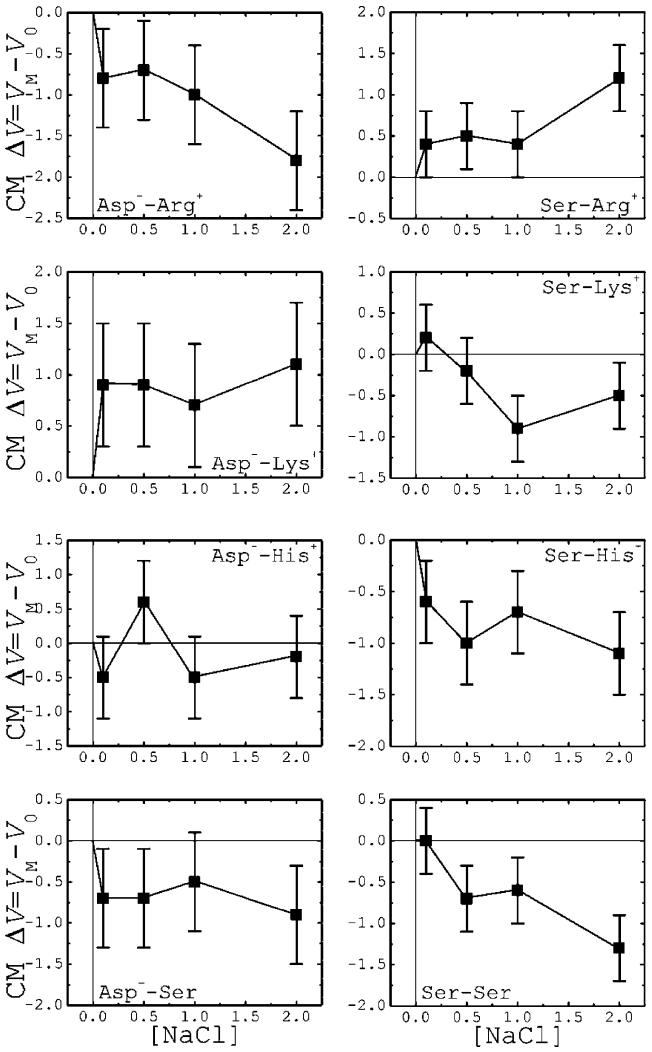

Figure 5. Changes (ΔV_M) of the PMF (in kcal/mol) at the contact distance (r_{cm}) as a function of [NaCl] (in M) for the eight dimers studied. The reference is pure water (error bars estimated as $\sigma\Delta V_M(r) \approx \sigma V_0(r) + \sigma V_M(r)$); negative values indicate stabilization of the dimer at the corresponding value of [NaCl].

solution and solvation shell to the forces and intermolecular potentials. To this end, the solvent forces ($F_{s,M}$) are decomposed into a bulk ($F_{b,M}$) and a solvation-shell ($F_{ss,M}$) term, i.e., $F_{s,M} = F_{b,M} + F_{ss,M}$. To carry out the calculation, a new trajectory was created out of the original dynamics containing only the coordinates of the water molecules and ions within 5 Å of any atom of the solute. The intermolecular PMF was then calculated from the new trajectory, which gave the solvation-shell contribution ($V_{ss,M}$) to the total PMF (V_M). With the above definition of solvation shell, the number of water molecules and ions in the system fluctuated in time, so long-range forces were calculated exactly. The bulk component to the PMF was then obtained as the difference $V_{b,M}(r) = V_M(r) - V_{ss,M}(r)$. Figure 1C shows $V_{b,M}(r)$ and $V_{ss,M}(r)$ for pure water and 2 M solution. The bulk component is mostly electrostatics and decreases with added salt, as expected. It also shows a quasi-linear behavior with the distance. By contrast, the solvation-shell component increases with the addition of salt. Moreover, the presence of ions in the solvation shell accentuates the changes in the slope of $V_{ss,M}$ within specific distance intervals: $r < 4.5$, $4.5 < r < 7.5$, $7.5 < r < 10$, and $r > 10$ Å (changes indicated by arrows). The figure shows that both bulk electrostatics and solvent-induced contributions are important in modulating the intermolecular interactions in the 0−2 M concentration range. However, adding salt amplifies the effects of the solvation shell substantially (see Discussion).

To further analyze the molecular origin of the changes in $\Delta V_2(r)$, the spatial structure of the salt-free solvent is analyzed. As the distance between the monomers increases, there is a restructuring of water around the solutes, whose changes can be characterized by analyzing the spatial distribution function (sdf) of the solvent.[45] For a given conformation of the solute, the sdf's are calculated as $g(\mathbf{r}) = \rho_w^{-1}\rho(\mathbf{r}) = \rho_w^{-1}\delta N(\mathbf{r})\delta V^{-1}$, where $\rho(\mathbf{r})$ is the number density of water molecules (water oxygen) at position $\mathbf{r}$; $\delta N(\mathbf{r})$ is the average number of water molecules within an element of volume δV centered at position $\mathbf{r}$, given by $\delta N(\mathbf{r}) = \tau^{-1} \int N(\mathbf{r},t)\, dt$, with $N(\mathbf{r},t) = \sum \delta(\mathbf{r} - \mathbf{r}_i(t))$, where the sum runs over all of the water molecules in the liquid, and $\delta(\mathbf{x})$ is 1 if $\mathbf{x} \subset \delta V$ and 0 otherwise; ρ_w is the bulk water number density ($\rho_w = 0.03325$ Å$^{-3} = M_w N_A$; $M_w \approx 55.5$ mol/liter is the water molar concentration, and N_A is the Avogadro number); the size of the volume element δV was chosen as a compromise between convergence (within τ) and error (σ) of $g(\mathbf{r})$ in bulk ($g_{bulk} = 1$), resulting in $\delta V = (0.65$ Å$)^3$ and $\sigma \approx 0.2$. Local maxima $g_m(\mathbf{r})$ were calculated numerically and deemed statistically significant if $g_m(\mathbf{r}) > 1.6$. Figure 6 shows the location of the peaks of $g(\mathbf{r})$ (red dots) for the solvent-separated distance $r = r_{ss} \approx 4.5$ Å and for $r = 7.5$ and 10 Å, i.e., the approximate intermolecular separations where the changes in the potentials and forces occur (the locations of arrows a−c in Figures 1B and 1C). The peaks are located at HB distances, r_p, (2.5 Å $< r_p <$ 3.5 Å) of each other or from an acceptor or donor atom of the dimer. A high degree of solvent structuredness is observed ($1.6 < g_m < 4$), which is dictated mainly by the symmetry of the side chains: the peaks are located in a tetrahedral-like distribution around each of the oxygen atoms of D and in the plane of the R side chain. As the monomers separate from each other (dimer dissociation), new peaks appear in the intervening space (cf. Figure 6); secondary maxima in the sdf's are also observed at r_p distances from the first peaks but not discussed here. The spatial distributions of the peaks around each solute change little with the intermolecular distance. They are similar to the distributions around isolated, fully hydrated solutes, which are recovered at large intermolecular separation, i.e., beyond the "rupture" point, $r = R_s$, where the interconnection of the peaks breaks down (R_s is different for each dimer; $R_s \approx 12$ Å for DR). These observations and Figure 1B suggest that the changes in ΔV_2 are related to the changes in the structure (values and spatial location of $g_m(\mathbf{r})$) and possibly dynamics (e.g., mean residence time) of the solvent in the region between the monomers.

The overall features described above for DR are observed in all the other dimers. However, quantitative differences are also evident that are unique to each case. Figures 2B−4B show $\Delta V_2(r)$ and $F_{s,M}(r)$ for SR, DS, and SS, while Figures 7−9 show the location of the corresponding sdf peaks (for $r < R_s$). Close inspection of these figures shows that $F_{s,2}$ decreases with respect to $F_{s,0}$ in the region $r_{cm} < r < r_{ss}$ in all cases; this behavior is also observed in DK (see below), DH, SK, and SH (not discussed here). Note, however, that the destabilization of the SR dimer at 2 M with respect to pure water (see $\Delta V_2(r)$ in Figure 2B) results mainly from changes in the relative magnitude and direction of the solvent forces at $r > r_{ss}$. Note that the solvent force above $r \approx 7.5$ Å is mostly repulsive in 2 M solution but attractive in pure water, which accounts for large part (∼1 kcal/mol) of the total destabilization of the dimer (∼1.2 kcal/mol). The sharp changes in ΔV_2 observed in the DR dimer are less pronounced in this case, although still appear about the same

TABLE 1: Effects of NaCl Salt Concentration on the Intermolecular Potentials of Mean Force in Polar/Charged Amino Acid Dimers at $T = 298$ K[a]

	Arg^+	Lys^+	His^+	Ser	[NaCl]
Asp^-	−0.8(0.6),−0.6(0.6),−0.3(0.6)	0.9(0.6),0.9(0.6),0.4(0.6)	−0.5(0.6),−0.3(0.6),−0.5(0.4)	−0.7(0.6),−0.5(0.4),−0.3(0.4)	0.1 M
	−0.7(0.6),−0.7(0.6),−0.5(0.6)	0.9(0.6),0.8(0.6),0.7(0.6)	0.6(0.6),0.7(0.6),0.6(0.4)	−0.7(0.6),−0.7(0.4),−0.5(0.4)	0.5 M
	−1.0(0.6),−0.7(0.6),−0.3(0.6)	0.7(0.6),0.7(0.6),0.5(0.6)	−0.5(0.6),−0.3(0.6),0.1(0.4)	−0.5(0.6),−0.2(0.4),−0.1(0.4)	1.0 M
	−1.8(0.6),−1.5(0.6),−1.0(0.6)	1.1(0.6),1.4(0.6),1.1(0.6)	−0.2(0.6),0.0(0.6),0.3(0.4)	−0.9(0.6),−0.8(0.4),−0.5(0.4)	2.0 M
Ser	0.4(0.4),0.4(0.4),0.2(0.4)	0.2(0.4),0.1(0.4),0.3(0.3)	−0.6(0.4),−0.4(0.4),−0.7(0.4)	0.0(0.4),0.2(0.3),0.4(0.3)	0.1 M
	0.5(0.4),0.6(0.4),0.5(0.4)	−0.2(0.4),−0.4(0.4),−0.2(0.3)	−1.0(0.4),−0.6(0.4),−0.8(0.4)	−0.7(0.4),−0.6(0.3),−0.2(0.3)	0.5 M
	0.4(0.4),0.6(0.4),0.6(0.4)	−0.9(0.4),−0.9(0.4),−0.6(0.3)	−0.7(0.4),−0.3(0.4),−0.1(0.4)	−0.6(0.4),−0.5(0.3),0.1(0.3)	1.0 M
	1.2(0.4),1.4(0.4),1.6(0.4)	−0.5(0.4),−0.7(0.4),−0.3(0.3)	−1.1(0.4),−0.9(0.4),−0.7(0.4)	−1.3(0.4),−1.2(0.3),−0.3(0.3)	2.0 M

[a] PMF differences $\Delta V_M(r) \equiv V_M(r) - V_0(r)$ at the contact (r_{cm}), transition state (r_{ts}), and solvent-separated (r_{ss}) proton−acceptor distances r; index 0 and M indicates pure water and solution at M molar NaCl concentration, respectively; values at r_{cm}, r_{ts}, and r_{ss} are given in the left, middle, and right entries (error estimates, $\sigma\Delta V(r) \approx \sigma V_0(r) + \sigma V_M(r)$, are in parentheses).

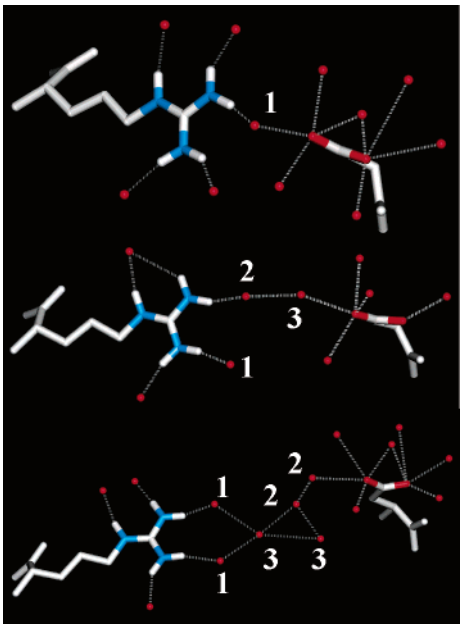

Figure 6. Peaks in the spatial distribution functions (sdf's) of pure water at three intermolecular distances: $r = r_{ss} = 4.6$ Å (upper panel; arrow a in Figure 1B), $r = 7.5$ Å (middle), and $r = 10$ Å (lower). Peaks connecting the side chains functional groups are labeled (m) in decreasing order of $g_m(\mathbf{r})$ (see text): upper panel, $g_1 = 3.7$; middle panel, $g_1 = 3.2$, $g_2 = 3.0$, $g_3 = 2.7$; lower panel, $g_1 = 2.7$, $g_2 = 1.9$, $g_3 = 1.7$ (error bars estimated as $\sigma[g_m] \approx 0.2$ in all cases). Only heavy atoms and polar hydrogens are displayed.

distances. For the DS dimer in pure water, the solvent exerts a repulsive force ($F_{s,0} > 0$) at all distances (inset in Figure 3B); however, increasing the salt concentration causes the solvent forces to become attractive ($F_{s,2} < 0$) when new sdf peaks form (at $r \approx 4.5$ and $r \approx 7.5$ Å). Only two peaks are observed in the solvent density around DS (cf. Figure 8); i.e., above $R_s \approx 8-9$ Å the monomers become independently hydrated. Figure 3B shows that in this case $\Delta V_2(r)$ increases steadily only in the region $r < r_{ss} \approx 4.5$ Å, which is sufficient to account for large part of the overall stabilization of the dimer. Similar behavior is observed for SS (cf. Figure 4B), where $\Delta V_2(r)$ undergoes significant changes ($>RT$) only at distances shorter than r_{ss}. However, in this case the tendency to stabilize the dimer begins at the position of the second peak at $r \approx 7.5$ Å rather than at the first peak at $r \approx 4.5$ Å as in DS; however, the appearance of the first peak produces a significant change in ΔV_2 of ~0.8 kcal/mol. As shown in the inset of Figure 4B, $F_{s,2}$ is not only less repulsive than $F_{s,0}$ in the region $r_{cm} < r < r_{ss}$ but is also more attractive for $r_{ss} < r < 7.5$ Å; the changes of the relative strengths/directions of the forces in both intervals account for most of the stabilization of the dimer.

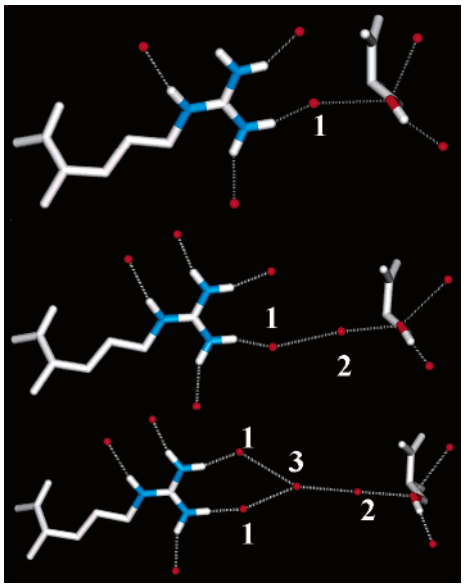

Figure 7. As in Figure 6 for Ser−Arg^+: upper panel, $g_1 = 3.4$; middle panel, $g_1 = 3.5$, $g_2 = 2.8$; lower panel, $g_1 = 3.0$, $g_2 = 2.8$, $g_3 = 1.6$.

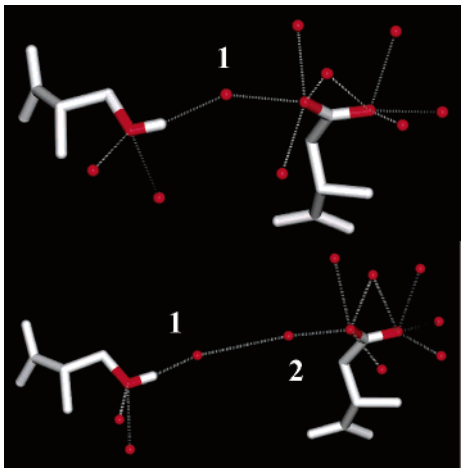

Figure 8. As in Figure 6 for Asp^-−Ser: upper panel, $g_1 = 3.8$; lower, $g_1 = 3.0$, $g_2 = 2.4$.

The observations above indicate that besides the electrostatic effects of bulk a subtle balance of forces operate on the solutes, which originates in the structure of the surrounding solvent (see Discussion). Further insight on these effects may be gained by analyzing the DR and DK dimers since the presence of salts elicits the opposite effects on their PMF (cf. Figure 5). Figure 10 shows ΔV_2 and $F_{s,M}(r)$ for DK. A comparison with Figure 1B reveals a similar up-and-down modulation of ΔV_2 as a function of r. However, the relative magnitudes of the decays

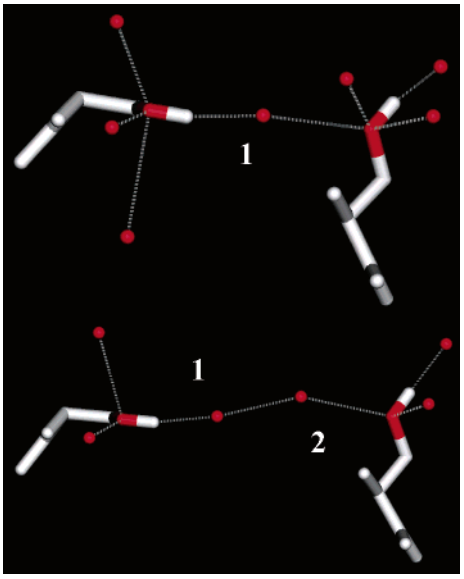

Figure 9. As in Figure 6 for Ser−Ser: upper panel, $g_1 = 3.8$; lower panel, $g_1 = 3.6$, $g_2 = 2.7$.

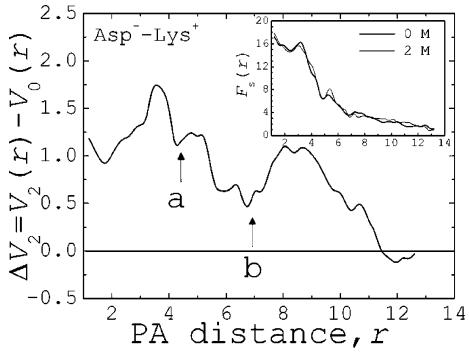

Figure 10. As in Figure 1B for $Asp^- - Lys^+$.

and growths in each interval result in an overall upward slope of ΔV_2, leading to ~1 kcal/mol destabilization, in contrast to DR. The magnitude of $F_{s,M}$ is larger in DK than in DR, although the solvent tends to dissociate the dimers in both cases ($F_{s,M} > 0 \; \forall \; r$). A comparison of the sdf between the two dimers reveals that the solvent is less structured in DK (not shown) than in DR and the solvent structure breaks down at $R_s \approx 8-9$ Å. In fact, R elicits the highest degree of structural order regardless of the interacting partner. The changes of $\Delta V_2(r)$ observed in 4.5 Å $< r <$ 7.5 Å for DK (Figure 10) are analogous to the changes observed in DR within the same region (Figure 1B). However, the relative magnitude of the decays and growths within this interval are quantitatively different. This difference leads to a ~1 kcal/mol stabilization of DR with respect to pure water, while slightly destabilizing DK (note that similar behavior is observed in Figure 3B for the DS dimer). Because of the remarkable contrast in the PMFs of these two dimers, it is instructive to analyze the restructuring of the spatial distribution of ions and water as they dissociate. A calculation of the sdf for Cl^- and Na^+ is then carried out; the calculations were performed as described above with $\rho_{ion} = 0.0012$ Å^{-3} at 2 M concentration. The analysis here is qualitative and carried out only for $r = 7.5$ Å, sufficient to illustrate the possible microscopic origin of the competing effects in these systems (see Discussion). Figure 11 shows the sdf of the ions around the dimers; $g(\mathbf{r})$ above an arbitrary cutoff is shown, which is the same for both ions for the sake of comparison. Ions in the hydration shells disrupt the structure of water and rearrange around the solutesas determined mainly by the topology of the

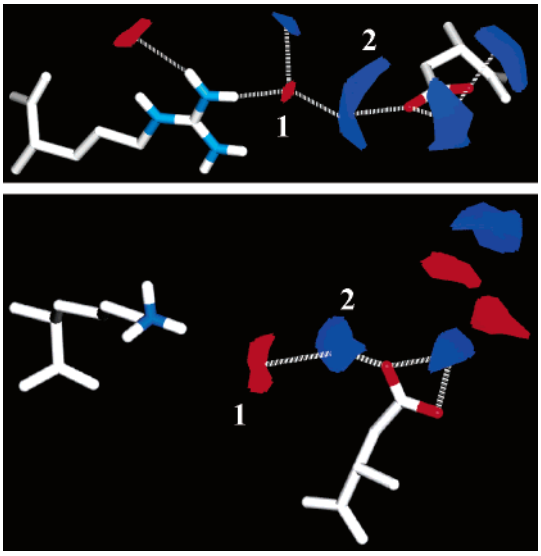

Figure 11. Spatial distribution functions (sdf's) of ions (red, Cl^-; blue, Na^+) around $Asp^- - Arg^+$ (upper panel) and $Asp^- - Lys^+$ (lower panel) at an intermolecular separation $r = 7$ Å (see Figures 1B and 10).

side chains. Thus, the chloride ions tend to distribute in the plane of arginine, whereas sodium ions tend to distribute around the oxygen atoms of the aspartate side chain; this distribution is similar to the distribution of water. The spatial distribution around the DR dimer (upper panel of Figure 11) suggests that ions entering the hydration shells may tend to position in pairs between the two monomers. The distance between the centers of the two local sdf lobes (labeled 1 and 2 in the upper panel) is ~3 Å; the distance between the center of lobe 1 and the closer hydrogen in R is ~2.3 Å, and between lobe 2 and the closer oxygen in D is ~2.2 Å. This arrangement possibly contributes to ion-pair-mediated DR interactions and explains the sensible decrease of the repulsive solvent force ($F_{s,2}$) and the local stabilization of this dimer (cf. Figure 1). By contrast, no such ion-pair density profile appears between the DK dimer (lower panel) that may explain a similar stabilization. The closest distance between the center of lobe 1 and a hydrogen of K is ~4.5 Å, while the distance between the centers of lobe 1 and 2 is ~2.4 Å, shorter than in DR. This suggests that K fails to recruit nearby Cl^- ions to the same extent that R does in the presence of D. As a consequence, D ends up bringing toward itself the ion pairs that enter its hydration shell. Therefore, no ion-pair-mediated interactions occur in DK, and the solvent force $F_{s,2}$ remains almost unchanged with respect to $F_{s,0}$ (cf. Figure 10). As a consequence, the stabilization provided by this interaction in the r~6−8 Å range in DR is not observed in DK, presumably by a compensation of water−solute and ion−solute forces. To quantify these forces and their competing effects, a systematic study of the different solvent contributions is needed (see Discussion).

Conclusions and Discussion

The effects of salts on the intermolecular potentials between polar/charged amino acid side chains have been studied quantitatively through systematic MD simulations. The strength of the interactions was shown to either increase or decrease with the addition of salt up to 2 M concentration. No obvious correlation was observed between the polar/charged nature of the interacting monomers and the extent of (de)stabilization of the dimers. The results show that a critical balance of solvent

forces operates on the solutes in the concentration range studied. The ions appear to affect the mean forces exerted on the solutes at specific intermolecular separations. The changes observed in the solvent forces occur when regions of high solvent density develop between the solutes as they dissociate. The solvent forces, $F_{s,M}$, shown in the insets of Figures 1B−4B can be partitioned into two terms: a bulk electrostatic contribution, $F_{b,M}$, and a nonbulk (solvation-shell) contribution, $F_{ss,M}$. Figure 1C shows that both components contribute significantly to the intermolecular potential, both in pure water and in solution. However, the relative magnitudes of the bulk and nonbulk contributions shift within the 0−2 M concentration range (at least in the DR dimer); while in pure water bulk electrostatics are more important than solvent-induced effects, the trend reverses at 2 M concentration. The bulk forces can be further partitioned into contributions from the ions, $F_{b,i,M}$, and from water, $F_{b,w,M}$. Similarly, the nonbulk forces can be separated into contribution from direct ion−solute interactions, $F_{ss,i,M}$, and from the hydration water, $F_{ss,w,M}$. Bulk forces ($F_{b,M}$) operate regardless of the salt concentration and provide for a basal modulation of the interactions (e.g., the Debye−Hückel theory[46] describes this effect in strong electrolytes). However, the results presented here show that nonbulk contributions are critical to define the outcome of the stabilization, particularly in the upper limits of salt concentrations (∼1−2 M). It would be of interest to study the behavior of each of the above contributions with the addition of salt. Such analysis would allow identification and quantitative characterization of the most important forces underlying molecular association/dissociation of small molecules in solution. A small ligand on a protein/solvent interface experiences the same kind of forces (and torques) discussed here; such interactions control the manner in which the ligand docks to the protein and determine the strength of the association. Prediction of ligand-binding modes and calculations of binding free energy are two basic goals in medicinal chemistry for the design or improvement of drugs. Insight into the molecular origins of solvent-induced interactions and their modulations by salts would have an obvious impact in the reliability of such calculations and predictions.

Finally, the prospect of describing the complex nonbulk effects of salts, i.e., quantifying $F_{ss,w,M}$ and $F_{ss,i,M}$, through a simplified picture that may only require knowledge of the location of sdf peaks (of water and ions) around the solutes may have other practical implications. Biological systems vary greatly in size and involve processes that may span several orders of magnitude. Realistic simulations of these systems using an atomistic description of all their constituents (solutes, salts, cosolvents, water, etc.) are computationally expensive. Besides, convergence and statistical significance of thermodynamic quantities extracted from such simulations may also require long simulations (possibly unrelated to the underlying biological process, e.g., calculation of binding free energy or prediction of ligand-binding modes). Replacing the atomistic description of part of the system by a continuum[47−49] would allow expansion of the scope of applicability of computer simulations to biological and chemical systems. Describing solvent-induced forces through a simple model that only accounts for the structure (and possibly dynamics) of water and ions in high-density regions around the solutes (e.g., using integral equation-based formalisms[50−53]) may help to incorporate into such continuum formulation an important component of the physics of the system that is required for meaningful calculations. Corrections for these effects in continuum approximations have largely been ignored (see discussion in refs 47 and 48), and efforts have been directed mainly to describing bulk electrostatic effects. A description of nonbulk effects is ultimately needed for incrementally improving the quality of continuum approximations.

Acknowledgment. This study utilized the high-performance computational capabilities of the Beowulf PC/Linux cluster at the National Institutes of Health (NIH) (http://biowulf.nih.gov). The simulations were performed in the Beowulf GNU/Linux cluster at the Center for Molecular Modeling (http://cmm.cit-.nih.gov). This research was supported by the Intramural Research Program of the NIH, through the Center for Information Technology, U.S. Department of Health and Human Services, Bethesda, Maryland.

References and Notes

(1) Makhatadze, G. I.; Privalov, P. L. *J. Mol. Biol.* **1993**, *232*, 639.
(2) Privalov, P. L.; Makhatadze, G. I. *J. Mol. Biol.* **1993**, *232*, 660.
(3) Reichardt, C. *Solvents and Solvent Effects in Organic Chemistry*, 3rd ed.; Wiley-VCH: Weinheim, Germany, 2002.
(4) Ben-Naim, A. *Biopolymers* **1990**, *29*, 567.
(5) Ben-Naim, A.; Ting, K. L.; Jernigan, R. L. *Biopolymers* **1990**, *29*, 901.
(6) Camacho, C. J.; Weng, Z. P.; Vajda, S.; DeLisi, C. *Biophys. J.* **1999**, *76*, 1166.
(7) Dixit, S.; Crain, J.; Poon, W. C. K.; Finney, J. L.; Soper, A. K. *Nature* **2002**, *416*, 829.
(8) Kumar, A. *Chem. Rev.* **2001**, *101*, 1.
(9) Carta, R.; Tola, G. *J. Chem. Eng. Data* **1996**, *41*, 414.
(10) Kohn, W. D.; Kay, C. M.; Hodges, R. S. *J. Mol. Biol.* **1997**, *267*, 1039.
(11) Lee, K. K.; Fitch, C. A.; Lecomte, J. T. J.; Garcia-Moreno, E. B. *Biochemistry* **2002**, *41*, 5656.
(12) Hamelink, J. M.; Rudolph, E. S. J.; van der Wielen, L. A. M.; Vera, J. H. *Biophys. Chem.* **2002**, *95*, 97.
(13) Brooks, C. L.; Nilsson, L. *J. Am. Chem. Soc.* **1993**, *115*, 11034.
(14) Robinson, D. R.; Jencks, W. P. *J. Am. Chem. Soc.* **1965**, *87*, 2470.
(15) Cacace, M.; Landau, E.; Ramsden, J. *Q. Rev. Biophys.* **1997**, *30*, 241.
(16) Kunz W.; Henle J.; W, N. B. *Curr. Opin. Colloid Interface Sci.* **2004**, *9*, 19.
(17) Collins, K.; Washabaugh, M. *Q. Rev. Biophys.* **1985**, *18*, 323.
(18) Rahman, A.; Stillinger, F. H. *J. Chem. Phys.* **1971**, *55*, 3336.
(19) Chandra, A. *Phys. Rev. Lett.* **2000**, *85*, 768.
(20) Geissler, P. L.; Dellago, C.; Chandler, D.; Hutter, J.; Parrinello, M. *Science* **2001**, *291*, 2121.
(21) Karplus, M.; McCammon, J. A. *Nat. Struct. Biol.* **2002**, *9*, 646.
(22) Garcia-Viloca, M.; Gao, J.; Karplus, M.; Truhlar, D. G. *Science* **2004**, *303*, 186.
(23) Warshel, A.; Aqvist, J. *Annu. Rev. Biophys. Biophys. Chem.* **1991**, *20*, 267.
(24) Warshel, A.; Papazyan, A. *Curr. Opin. Struct. Biol* **1998**, *8*, 211.
(25) Sharp, K.; Fine, R.; Honig, B. *Science* **1987**, *236*, 1460.
(26) Elcock, A. H.; Gabdoulline, R. R.; Wade, R. C.; McCammon, J. A. *J Mol Biol* **1999**, *291*, 149.
(27) Selzer, T.; Albeck, S.; Schreiber, G. *Nat. Struct. Biol.* **2000**, *7*, 537.
(28) Lee, L. P.; Tidor, B. *Nat. Struct. Biol.* **2001**, *8*, 73.
(29) Bruge, F.; Fornilli, S. L.; Malenkov, G. G.; Palma-Vittorelli, M. B.; Palma, M. U. *Chem. Phys. Lett.* **1996**, *254*, 283.
(30) Ben-Naim, A. *J. Phys. Chem.* **1990**, *94*, 6893.
(31) Chandler, D. *Nature* **2002**, *417*, 491.
(32) Lum, K.; Chandler, D.; Weeks, J. D. *J. Phys. Chem. B* **1999**, *103*, 4570.
(33) TenWolde, P. R.; Chandler, D. *Proc. Natl. Acad. Sci. U.S.A.* **2002**, *99*, 6539.
(34) Sundberg, E. J.; Urrutia, M.; Braden, B. C.; Isern, J.; Tsuchiya, D.; Fields, B.; Malchiodi, E. L.; Tormo, J.; Schwarz, F.; Mariuzza, R. A. *Biochemistry* **2000**, *39*, 15375.
(35) Baldwin, R. L. *Science* **2002**, *295*, 1657.
(36) Dzubiella, J.; Hansen, J.-P. *J. Chem. Phys.* **2003**, *119*, 12049.
(37) Durell, S. R.; Brooks, B. R.; Ben-Naim, A. *J. Phys. Chem.* **1994**, *98*, 2198.
(38) Ben-Naim, A. *J. Chem. Phys.* **1990**, *93*, 8196.
(39) Christenson, H. K.; Fang, J. F.; Ninham, B. W.; Parker, J. L. *J. Phys. Chem.* **1990**, *94*, 8004.
(40) Kokkoli, E.; Zukoski, C. F. *Langmuir* **1998**, *14*, 1189.
(41) Mancera, R. L. *J. Phys. Chem. B* **1999**, *103*, 3774.
(42) Ghosh, T.; Kalra, A.; Garde, S. *J. Phys. Chem. B* **2005**, *109*, 642.

(43) Hassan, S. A. *J. Phys. Chem. B* **2004**, *108*, 19501.
(44) Brooks, B. R.; Bruccoleri, R. E.; Olafson, B. D.; States, D. J.; Swaminathan, S.; Karplus, M. *J. Comput. Chem.* **1983**, *4*, 187.
(45) Kusalik, P. G.; Svishchev, I. M. *Science* **1994**, *265*, 1219.
(46) Pathria, R. K. *Statistical Mechanics*; International Series of Monographs in Natural Philosophy 45; Pergamon Press: New York, 1972.
(47) Hassan, S. A.; Mehler, E. L. *Int. J. Quantum Chem.* **2005**, *102*, 986.
(48) Li, X.; Hassan, S. A.; Mehler, E. L. *Proteins* **2005**, *60*, 464.
(49) Tomasi, J.; Mennucci, B.; Cammi, R. *Chem. Rev.* **2005**, *105*, 2999.
(50) Hansen, J. P.; McDonald, I. R. *Theory of Simple Liquids*; Academic: London, 1976.
(51) Chandler, D.; McCoy, J. D.; Singer, S. J. *J. Chem. Phys.* **1986**, *85*, 5971.
(52) Imai, T.; Kovalenko, A.; Hirata, F. *Chem. Phys. Lett.* **2004**, *395*, 1.
(53) Beglov, D.; Roux, B. *J. Phys. Chem. B* **1997**, *101*, 7821.